Vibration Suppression in High-speed Trains with Negative Stiffness Dampers

Xiang SHI[1, 2,a], Songye ZHU[* 2,b], Yi-qing NI[2,c], Jianchun Li[3,c]

[1] College of Information and Control Engineering, China University of Petroleum (East China), Qingdao, Shandong Province, China
[2] Department of Civil and Environmental Engineering, National Rail Transit Electrification and Automation Engineering Technology Research Center (Hong Kong Branch), The Hong Kong Polytechnic University, Hung Hom, Kowloon, Hong Kong
[3] Centre for Built Infrastructure Research, Faculty of Engineering and Information Technology, University of Technology Sydney, NSW, Australia
* Corresponding author: songye.zhu@polyu.edu.hk

(Received keep as blank , Revised keep as blank , Accepted keep as blank)

Abstract. This work proposes and investigates re-centering negative stiffness dampers (NSDs) for vibration suppression in high-speed trains. The merit of the negative stiffness feature is demonstrated by active controllers on a high-speed train. This merit inspires the replacement of active controllers with re-centering NSDs, which are more reliable and robust than active controllers. The proposed damper design consists of a passive magnetic negative stiffness spring and a semi-active positioning shaft for re-centering function. The former produces negative stiffness control forces, and the latter prevents the amplification of quasi-static spring deflection. Numerical investigations verify that the proposed re-centering NSD can improve ride comfort significantly without amplifying spring deflection.

Keywords: negative stiffness, vibration control, high-speed train, active control, re-centering

1. Introduction

High-speed trains as efficient and economical transportation tools have developed rapidly in the past decade. However, increasing train speed results in serious vibrations, which exert adverse effects on ride stability and quality. Therefore, vibration suppression in high-speed trains has become a crucial and challenging issue. Various control techniques for train suspension systems have been proposed to improve ride comfort and safety, and these techniques can be classified as passive, active, and semi-active. Passive control techniques possess relatively high reliability, robustness, and practicability, but their control performance is often limited because they cannot adapt to a wide frequency range of excitations induced by rail track irregularities.

Active control techniques can produce favorable control forces through actuators and exhibit high vibration suppression performance over a broad frequency range of excitations. Therefore, train suspensions have been investigated with various active control techniques (Yoshimura et al., 1993; Sasaki et al., 1994; Shimamune and Tanifuji, 1995; Pratt and Goodall, 1997; Goodall, 1997; Pearson et al., 1998; Tanifuji, 1998; Bruni and Resta, 2001; Goodall and Kortüm, 2002; Tanifuji et al., 2002; Peiffer et al., 2004; He and McPhee, 2005; Bruni et al., 2007; Orukpe et al., 2008; Mellado et al., 2009; Zhou et al., 2010; Orvnäs et al., 2011; Li et al., 2015). Active control requires a complicated system that involves sensors, actuators, controllers, external power supplies, and high initial and maintenance costs. Any measurement noise from sensors or power outage adversely affects control performance.

Meanwhile, semi-active control techniques based on magnetorheological (MR) dampers have been developed for train suspensions because their performance is better than that of passive control techniques, and their power requirement and cost are lower than those of active control techniques. Representative control strategies include skyhook control (O'Neill and Wale, 1994), neuro-fuzzy control (Atray and Roschke, 2004), adaptive fuzzy control (Yang et al., 2006), linear quadratic Gaussian (LQG) control (Liao and Wang, 2003; Wang and Liao, 2009a; b), and H^{∞} control (Zong et al., 2013). Moreover, Li et al. (2013) proposed a viscoelastic model of MR dampers and applied it in a high-speed train. Ni et al. (2016) tested the performance of MR dampers on a full-scale high-speed train. However, semi-active MR dampers can only provide control forces in the opposite direction of damper velocity and thus cannot fully identify the force–displacement relationship determined by active control strategies.

Several studies on active control have revealed that the linear quadratic regulator (LQR) algorithm, a commonly adopted optimal control theory for active dampers, may produce a damper force–displacement relationship with an apparent negative stiffness feature that benefits vibration control performance (Iemura and Pradono, 2005). Therefore, the negative stiffness concept has been increasingly applied

*Corresponding author, Associate Professor
E-mail: songye.zhu@polyu.edu.hk
[a] Research Associate
[b] Associate Professor
c Professor

in vibration control for different mechanical and civil structures, including high-speed trains (Lee and Goverdovskiy, 2012; Lee et al., 2016), vehicle seats (Lee et al., 2007; Le and Ahn, 2011), isolation tables (Platus and Ferry, 2007; Yang, 2013;), adjustable constant force systems (Liu et al., 2016), tunable stiffness systems (Churchill et al., 2016), buildings (Asai et al., 2013; Iemura et al., 2006; Iemura and Pradono, 2009; Pasala et al., 2012; Sun et al., 2017), stay cables (Li et al., 2008; Weber and Boston, 2011, Shi et al., 2016; 2017; Balch et al., 2017), and cable-stayed bridges (Iemura and Pradono, 2002).

Inspired by these findings, various negative stiffness dampers (NSDs) have been developed through semi-active (Iemura and Pradono 2002, Iemura et. al. 2006; Høgsberg, 2011; Weber et al., 2011) or passive (Dijkstra et al. 1988; Lee et al. 2007; Iemura and Pradono, 2009; Pasala et al., 2012; Kalathur and Lakes, 2013; Cortes et. al., 2017) means. For example, Shi and Zhu (2015, 2017) recently proposed two passive designs of magnetic NSDs (MNSDs) that efficiently integrate the magnetic negative-stiffness mechanism and eddy-current damping in compact cylindrical configurations and developed corresponding optimal design methods. Passive or semi-active NSDs demonstrate superior control performance that is comparable to that of active controllers and are thus promising control strategies that present high performance and good reliability and practicability.

The feasibility of applying the negative stiffness mechanism in high-speed trains to improve ride comfort has also been investigated. To increase isolation efficiency at a low frequency range, which is harmful to humans, Lee and Goverdovskiy (2012) designed geometrically similar redundant mechanisms with negative stiffness that can be inserted into multi-stages of high-speed rails, including vehicle seats, bogies, and track beds. The effectiveness of their design was verified using vehicle seats (Lee and Goverdovskiy, 2012) and train bogies (Lee et al., 2016). Another study discovered that a decreasing suspension stiffness value may increase the critical speed of high-speed trains (Sun et al., 2013). A negative-stiffness spring is an efficient means to decrease suspension stiffness without compromising the carrying capacity. However, the effectiveness of NSDs in high-speed train suspensions has not been systematically examined. This work presents the benefits of negative stiffness behavior in vibration control for high-speed trains. Numerical simulations of active controllers in high-speed trains reveal a control force–displacement relationship with an apparent negative stiffness feature. Subsequently, a re-centering NSD is proposed and analyzed in parallel with train suspensions. The proposed NSD consists of a passive magnetic negative stiffness spring and a semi-active positioning shaft with a re-centering function. Numerical simulation results in different conditions indicate that the re-centering NSD can improve ride comfort effectively and prevent the amplification of suspension deflection. As low-bandwidth control strategies, re-centering NSDs are a simple and promising alternative to conventional active controllers.

2. Simulation of High-speed Trains

2.1 Dynamic Model of High-speed Trains

The model with 17 degrees of freedom (DOF) for high-speed trains proposed by Zong et al. (2013) is adopted for numerical simulations in this study. Fig. 1 shows the analytical model of a high-speed train with dampers. The high-speed train model in the figure is composed of one car body, two bogies, and four wheelsets. The car body is connected to the leading and rear bogies by secondary suspensions, and each bogie is connected to two wheelsets by primary suspensions (Zong et al., 2013). The dampers are installed in the secondary suspensions in the lateral direction because secondary lateral damping is the most critical element of a car body in terms of vibration suppression (Sun et al. 2013). As shown in Fig. 1, four dampers are installed; two of them symmetrically connect the car body and leading bogie, and the other two connect the car body and rear bogie. Table 1 lists the 17 DOFs considered in the high-speed train model, and the corresponding governing equations are briefly described in the Appendix.

The governing equations of the 17-DOF model can be expressed in the following matrix form.

$$\mathbf{M}\ddot{\mathbf{q}} + \mathbf{C}\dot{\mathbf{q}} + \mathbf{K}\mathbf{q} = \mathbf{F}_\mathbf{u}\mathbf{u} + \mathbf{F}_\mathbf{w}\mathbf{w} \tag{1}$$

where **M**, **C**, and **K** are the mass, damping, and stiffness matrices of a high-speed train, respectively; $\mathbf{F_u}$ is the coefficient matrix related to the locations of dampers or control devices; $\mathbf{F_w}$ is the excitation matrix due to track irregularities; and **q** is the vector containing all the DOFs of the train model.

$$\mathbf{q} = \begin{bmatrix} y_c & \varphi_c & \theta_c & y_{t1} & \varphi_{t1} & \theta_{t1} & y_{t2} & \varphi_{t2} & \theta_{t2} & ,\ldots \\ \ldots & y_{w1} & \varphi_{w1} & y_{w2} & \varphi_{w2} & y_{w3} & \varphi_{w3} & y_{w4} & \varphi_{w4} & \end{bmatrix}^{\mathrm{T}} \tag{2}$$

The vector of the control forces, **u**, is expressed as follows:

$$\mathbf{u} = \begin{bmatrix} u_1 & u_2 \end{bmatrix}^{\mathbf{T}} \tag{3}$$

where u_1 and u_2 are the control forces between the car body and leading bogie and between the car body and rear bogie, respectively. Each represents the resultant forces of the two symmetrically installed dampers.

$\mathbf{w}=[\mathbf{w_1}\,\mathbf{w_2}]^{\mathrm{T}}$ is the vector of track irregularities that excite the wheels, and $\mathbf{w_1}$ and $\mathbf{w_2}$ are track irregularities in lateral alignment (y_a) and cross level (θ_{cl}). They are defined as

$$\begin{aligned} \mathbf{w}_1 &= \begin{bmatrix} y_{a1} & y_{a2} & y_{a3} & y_{a4} & \theta_{cl1} & \theta_{cl2} & \theta_{cl3} & \theta_{cl4} \end{bmatrix}^{\mathrm{T}} \\ \mathbf{w}_2 &= \begin{bmatrix} \dot{y}_{a1} & \dot{y}_{a2} & \dot{y}_{a3} & \dot{y}_{a4} & \dot{\theta}_{cl1} & \dot{\theta}_{cl2} & \dot{\theta}_{cl3} & \dot{\theta}_{cl4} \end{bmatrix}^{\mathrm{T}} \end{aligned} \tag{4}$$

The calculation of lateral alignment and cross level is explained in detail in the next section.

The governing equations can be rewritten into a state space form as

$$\dot{\mathbf{z}} = \mathbf{A}\mathbf{z} + \mathbf{B}_\mathbf{c}\mathbf{u} + \mathbf{B}_\mathbf{w}\mathbf{w} \tag{5}$$

where **z** is the state vector,

$$\mathbf{z} = \begin{bmatrix} \mathbf{q} \\ \dot{\mathbf{q}} \end{bmatrix} \tag{6}$$

A is the state matrix,

Table 1 Late

Car body	Roll
Bogie	θ_c
	θ_{t1}
Wheelset	θ_{t2}

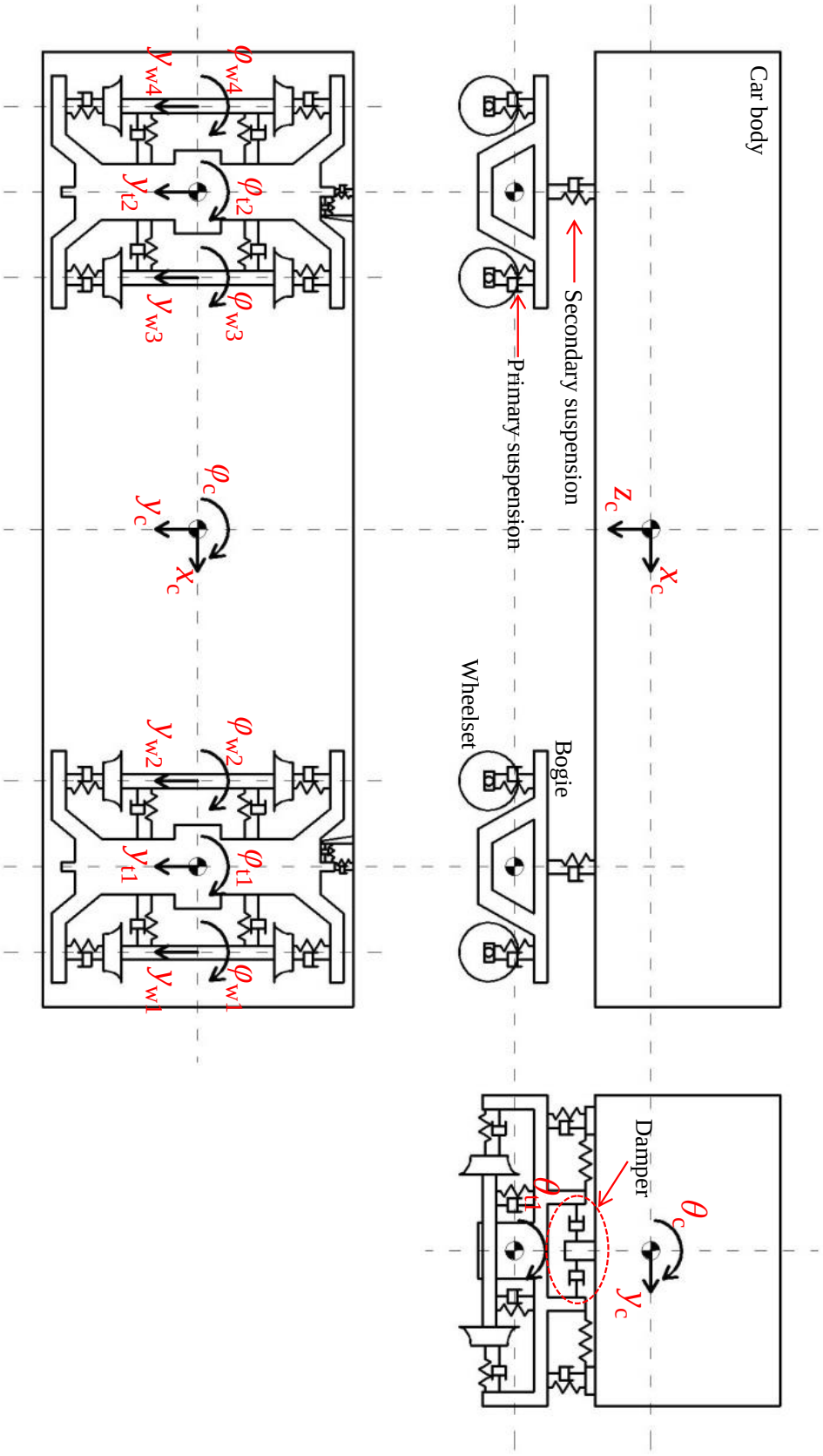

Fig. 1 Analytical model of a high-speed train with dampers (Zong et al., 2013)

$$\mathbf{A} = \begin{bmatrix} \mathbf{0} & \mathbf{I} \\ -\mathbf{M}^{-1}\mathbf{K} & -\mathbf{M}^{-1}\mathbf{C} \end{bmatrix} \quad (7)$$

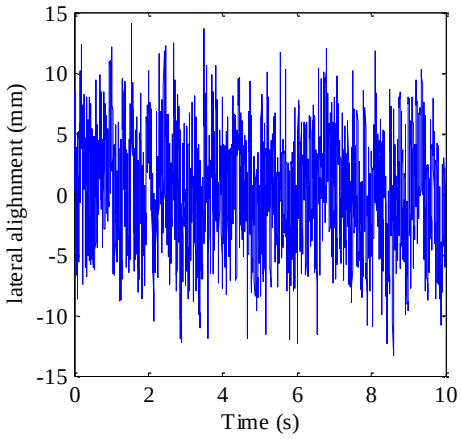

(a) Time history

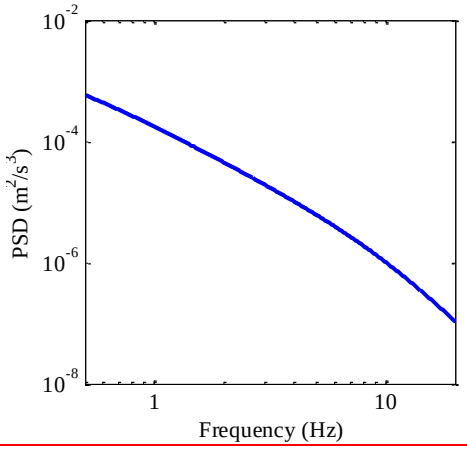

(b) PSD

Fig. 2 Lateral alignment of track irregularity

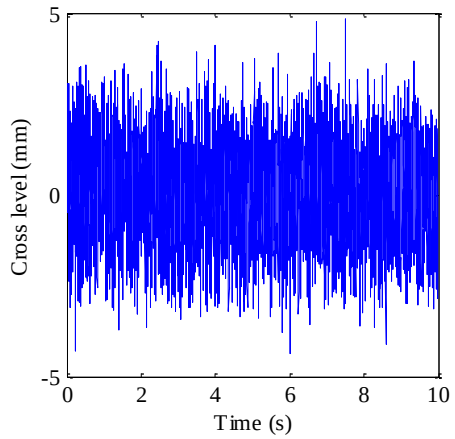

(a) Time history

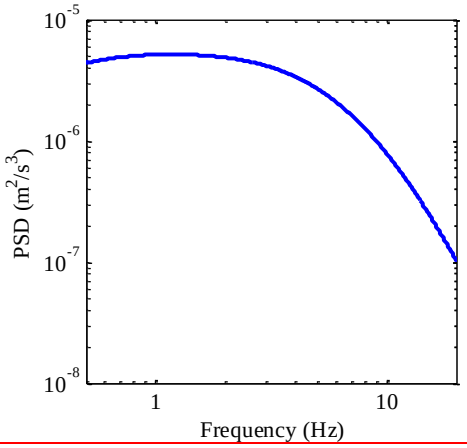

(b) PSD

Fig. 3 Cross level of track irregularity

$\mathbf{B}_w$ is the input matrix for track irregularities,

$$\mathbf{B}_w = \begin{bmatrix} \mathbf{0} \\ \mathbf{M}^{-1}\mathbf{F}_w \end{bmatrix} \quad (8)$$

and $\mathbf{B}_c$ is the input matrix for the damper forces,

$$\mathbf{B}_c = \begin{bmatrix} \mathbf{0} \\ \mathbf{M}^{-1}\mathbf{F}_u \end{bmatrix} \quad (9)$$

2.2 Track Irregularities

The vibrations of high-speed trains are mainly excited by geometrical irregularities of tracks. A simulation approach for track irregularities was established by Zong et al. (2013). Track irregularities occur in the vertical profile, cross level, lateral alignment, and gauge. The irregularities in lateral alignment and cross level are the main causes of the lateral vibrations of high-speed trains, and these two regularities can be calculated as (Garivaltis et al., 1980; Bhatti and Garg, 1984)

$$y_a = \frac{y_l + y_r}{2}, \quad \theta_{cl} = \frac{z_l + z_r}{2b} \quad (10)$$

where y_l and y_r are the lateral track irregularities of the left and right rails, respectively; z_l and z_r are the vertical track irregularities of the left and right rails, respectively; and b is half of the reference distance between the rails.

Track irregularities can be typically described by the power spectral densities (PSDs) of measurement data. According to Claus and Schiehlen (1998), the one-sided PSD functions of lateral alignment and cross level are given by

$$S_a = \frac{A_a \Omega_c^2}{\left(\Omega^2 + \Omega_r^2\right)\left(\Omega^2 + \Omega_c^2\right)}$$
$$S_c = \frac{\left(A_v / b^2\right)\Omega_c^2 \Omega^2}{\left(\Omega^2 + \Omega_r^2\right)\left(\Omega^2 + \Omega_c^2\right)\left(\Omega^2 + \Omega_s^2\right)} \quad (11)$$

where Ω is the spatial frequency (rad/m); Ω_c, Ω_r, and Ω_s are the truncated wavenumbers (rad/m); and A_a and A_v are two scalar factors of track irregularities.

Track irregularities in the time domain can be converted from PSD functions using the method proposed by Chen and Zhai (1999). Fig. 2 and Fig. 3 show the simulated track irregularities in the lateral alignment and cross level,

respectively. Fig. 2(a) and Fig. 3 (a) present the time histories, and Fig. 2(b) and Fig. 3(b) present the corresponding PSDs.

2.3 Curved Track

When a high-speed train travels on a curved track, the car body moves laterally due to a centrifugal force. Fig. 4(a) presents the geometric curvature of a curved track with a radius of 3200 m. The transition segment from a straight track to a circular one is 200 m long. When a high-speed train passes the curved track at 300 km/h, the corresponding centripetal acceleration is shown in Fig. 4(b).

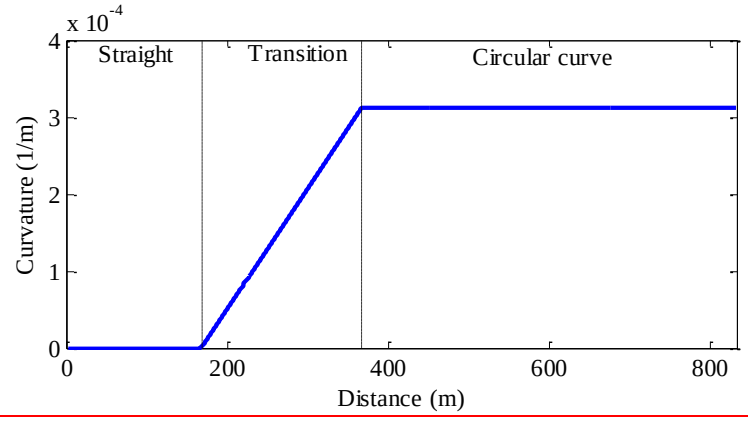

(a) Track geometry

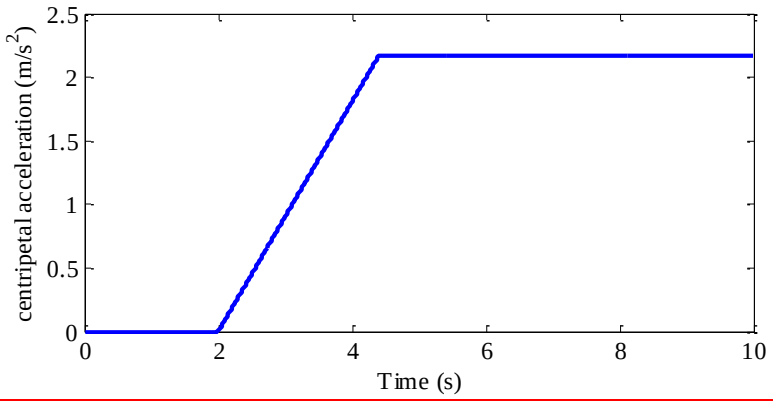

(b) Centripetal acceleration

Fig. 4 Curved track with a radius of 3,200 m

3. Negative Stiffness in Active Control

To verify the benefits of negative stiffness, the force–displacement relationship of the LQR controller for high-speed trains is investigated in this section.

The control forces of LQR controllers can be calculated as

$$\mathbf{u}_{lqr} = -\mathbf{G}_{lqr}\mathbf{z} \quad (12)$$

where $\mathbf{G}_{lqr}$ is the optimal feedback gain that minimizes quadratic performance index J.

$$J = \int_0^\infty \left(\mathbf{z}^T \mathbf{Q} \mathbf{z} + \mathbf{u}_{lqr}^T \mathbf{R} \mathbf{u}_{lqr} \right) dt \quad (13)$$

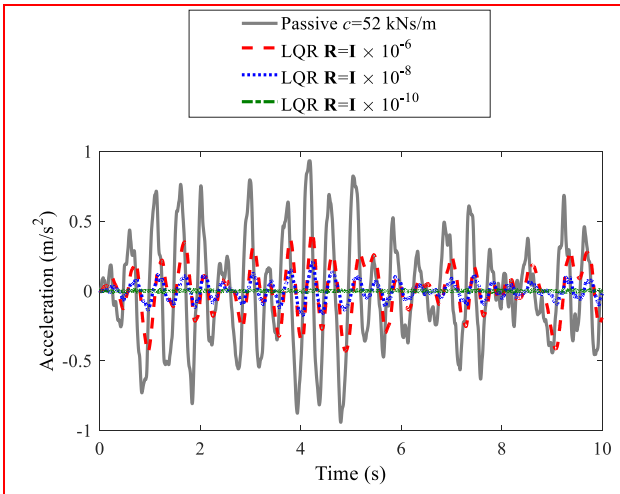

(a) Lateral accelerations

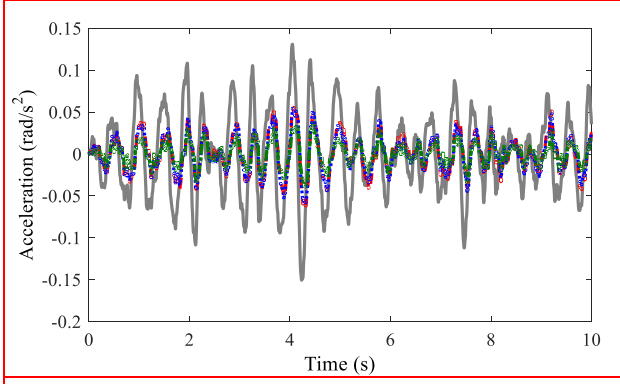

(b) Yaw accelerations

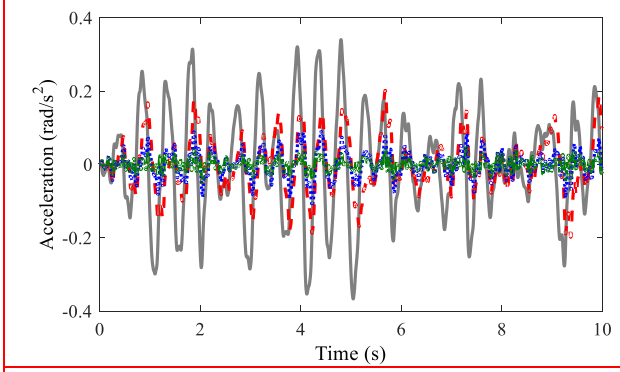

(c) Roll accelerations

Fig. 5 Time history of car body accelerations under random track irregularities

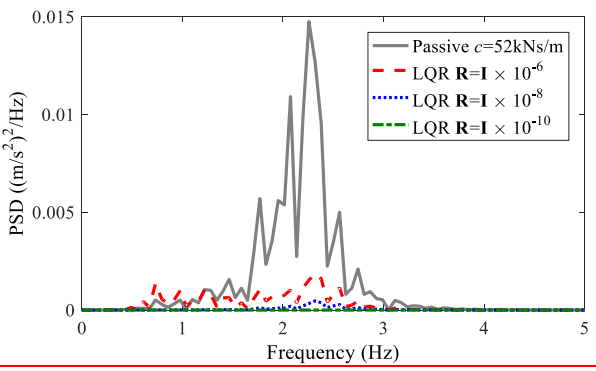

(a) Lateral accelerations

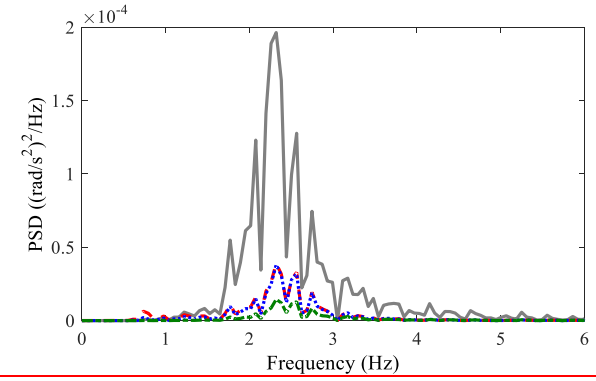

(b) Yaw accelerations

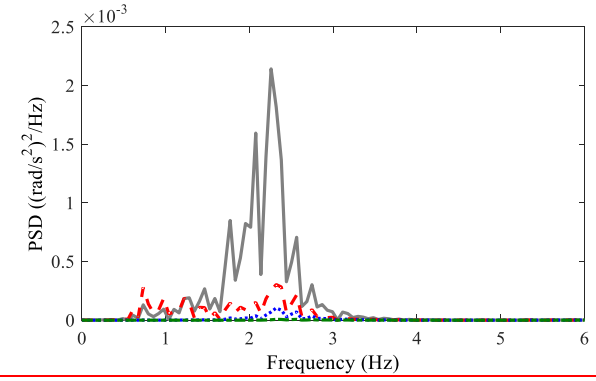

(c) Roll accelerations

Fig. 6 PSD of car body accelerations under random track irregularities

where **Q** and **R** are symmetric positive-definite matrices. Consequently, feedback gain $\mathbf{G}_{\mathbf{lqr}}$ can be determined as

$$\mathbf{G}_{\mathrm{lqr}} = \mathbf{R}^{-1}\mathbf{B}_{\mathbf{c}}^{T}\mathbf{P} \tag{14}$$

where **P** should satisfy the reduced-matrix Riccati equation

$$\mathbf{A}^{T}\mathbf{P} + \mathbf{P}\mathbf{A} - \mathbf{P}\mathbf{B}_{\mathbf{c}}\mathbf{R}^{-1}\mathbf{B}_{\mathbf{c}}^{T}\mathbf{P} + \mathbf{Q} = \mathbf{0} \tag{15}$$

By substituting Eq. (12) into Eq. (5), the state space equation of a high-speed train with LQR controllers can be expressed as

$$\dot{\mathbf{z}} = \left(\mathbf{A} - \mathbf{B}_{\mathbf{c}}\mathbf{G}_{\mathbf{lqr}}\right)\mathbf{z} + \mathbf{B}_{\mathbf{w}}\mathbf{w} \tag{16}$$

The performance of the LQR controller is determined by the **Q** and **R** matrices. Given that ride comfort is the focus of this work, the elements corresponding to car body vibration should be significantly larger than the rest. Given a **Q** matrix, the performance of the LQR controller can be manipulated by adjusting the **R** value. The control energy of the LQR controller generally increases as the **R** value decreases.

When a high-speed train with an LQR controller travels on a straight track at 300 km/h, its dynamic responses can be calculated from the state space model. The responses of the high-speed train with a passive damper (viscous damping: 52 kNs/m) are also calculated for reference. Fig. 5 and Fig. 6

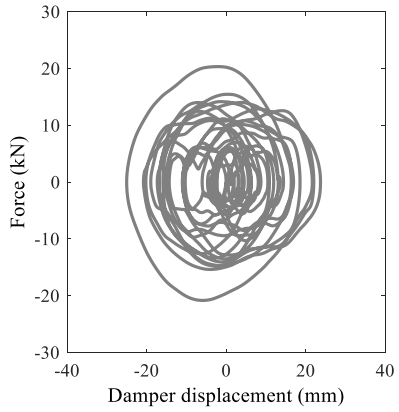

(a) Lead

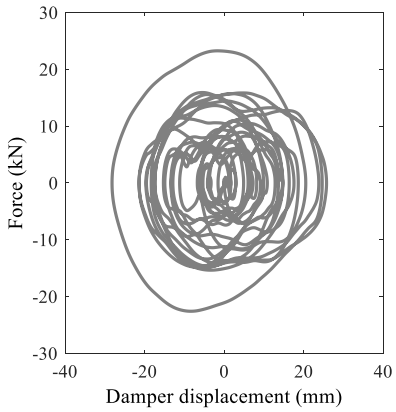

(b) Rear

Fig. 7 Control force vs. damper displacement of the passive viscous damper

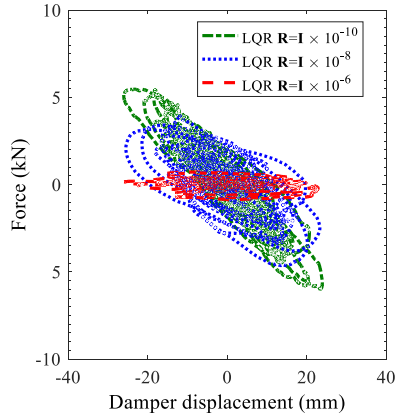

(a) Lead

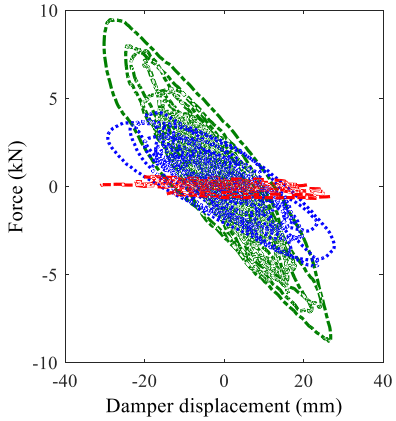

(b) Rear

Fig. 8 Control force vs. damper displacement of LQR

present the car body responses in time and frequency domains, respectively.

The performance of the LQR controller is generally much better than that of the passive damper, and the performance of the LQR controller improves as **R** decreases. When the train is protected by a passive damper, the root mean square (RMS) values of car body accelerations in the lateral, yaw, and roll directions are 0.381 m/s^2, 0.0499 rad/s^2, and 0.146 rad/s^2, respectively; when the LQR controller ($\mathbf{R} = \mathbf{I} \times 10^{-6}$) is adopted, the RMS values of car body accelerations in the lateral, yaw, and roll directions decrease to 0.176 m/s^2, 0.0225 rad/s^2, and 0.0755 rad/s^2, respectively. If $\mathbf{R} = \mathbf{I} \times 10^{-8}$, the RMS values in the lateral, yaw, and roll directions decrease to 0.0661 m/s^2, 0.0215 rad/s^2, and 0.0350 rad/s^2, respectively. If **R** is further decreased to $\mathbf{I} \times 10^{-10}$, the RMS values of car body accelerations in the lateral, yaw, and roll directions can be further reduced to 0.00193 m/s^2, 0.00211 rad/s^2, and 0.00441 rad/s^2, respectively (Fig. 5(a), 5(b), and 5(c)). Similar conclusions can also be drawn from the car body response in the frequency domain. As shown in Fig. 6(a), 6(b), and 6(c), the peak responses of PSD in the lateral, yaw, and roll directions decrease as the **R** value of the LQR controller decreases.

Fig. 7 and Fig. 8 present the force versus damper displacement relationship of the passive damper and LQR controllers, respectively. As shown in Fig. 7(a) and 7(b), no stiffness feature is observed in the force versus damper displacement relationship of leading and rear passive dampers. However, a significant negative stiffness feature is found in the force versus damper displacement relationship of leading and rear LQR controllers (Fig. 8(a) and 8(b)). As presented in Fig. 8, negative stiffness becomes increasingly significant as **R** decreases. The force versus damper displacement relationship of the LQR controller indicates that negative stiffness is beneficial in improving ride comfort in high-speed trains.

4. Re-centering NSD

Combining the high performance of active controllers and the high robustness of passive dampers is advantageous. A re-centering NSD is proposed in this work to replace the LQR controller. Magnetic negative stiffness is used to imitate the negative stiffness feature observed in the active controller, and the re-centering function is adopted to avoid large spring deflection of secondary suspensions.

4.1 Magnetic Negative Stiffness

Fig. 9 presents the conceptual design of the re-centering NSD for high-speed trains. The negative stiffness mechanism

of the proposed damper follows the principle of Design B MNSD (Shi and Zhu, 2015). The damper consists of one repositioning shaft and two magnets (one outer static magnet ring and one inner moving magnet cylinder with the same pole orientation). As shown in Fig. 10, when the two magnets are concentric, the moving magnet is at zero damper displacement. When the inner moving magnet moves away from the zero position, the repelling force between the two magnets is counterbalanced by an external force in the opposite direction of the displacement, which induces negative stiffness behavior (Shi and Zhu, 2015). The detailed design and optimization method of MNSD were developed by Shi and Zhu (2017).

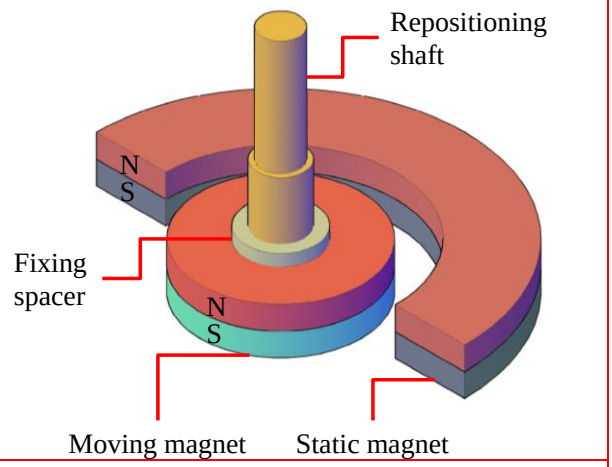

Fig. 9 Re-centering negative stiffness damper

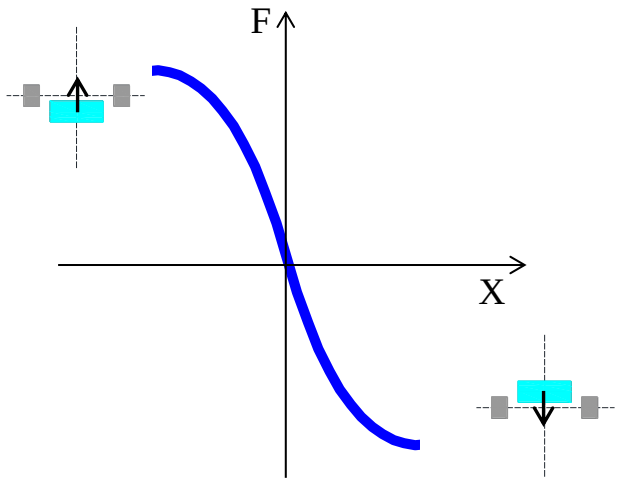

Fig. 10 Principle of negative stiffness

4.2 Re-centering Function

The re-centering function can prevent large spring deflection when high-speed trains with NSD travels on curved tracks. The re-centering function uses low-pass filtered lateral accelerations as the reference signal. Such a re-centering function belongs to low-bandwidth control because the reference signal is utilized to detect the low-frequency component of track inputs (e.g., curvature). A similar low-bandwidth control method, namely, Hold-Off-Device, has been implemented in high-speed trains (Allen, 1994; Orvnäs et al., 2010; 2011).

Fig. 11 shows the principle of the re-centering function in high-speed trains. As shown in Fig. 11(a), when a high-speed train travels on a straight track, its car body and bogie are symmetric. However, when the train passes a curved track, a quasi-static relative displacement (Δx) is generated by the centripetal acceleration in the lateral direction (Fig. 11(b)). This centripetal acceleration is measured by sensors with a low-pass filter; then, the controller sends control signals to actuators to re-center the damper (Fig. 11). If the re-positioning shaft of the left NSD elongates (Δx) and the shaft of the right NSD shortens (Δx), the relative position between the dampers' zero displacement and the centerline of the car body will not change. The relative displacement between the car body and bogie will not be amplified by the negative stiffness because the quasi-static loads are carried by the lateral stiffness of the train suspension. In practice, actuators could be a linear motor, a rotary motor with a ball screw, or a rotary motor with pinion and rack.

Aside from re-centering of NSD, HOD can also be adopted to minimize spring deflection. HOD is used to center the car body when a train travels on a curved track. As a result, bump stop contact between the car body and bogie is avoided. HOD was proposed by Allen (1994). Orvnäs et al. (2010, 2011) verified the effectiveness of HOD numerically and experimentally. In their implementation, the low-pass filtered lateral acceleration from the leading bogie was used as the reference signal, and this signal was multiplied by half the car body mass to create an actuator force that counteracts the lateral movement of the car body when a train travels on a curved track.

5. Performance Evaluation

5.1 Evaluation Cases

In this section, the performance of the re-centering NSD is evaluated with three different levels of negative stiffness. The negative stiffness values considered are −105, −210, and −315 kN/m, and each value represents the summation of the negative stiffness values provided by two symmetrically installed NSDs (Fig. 1). Therefore, each NSD is designed to provide only half of the target negative stiffness. We follow the design procedure developed by Shi and Zhu (2017), and the designed magnet dimensions that satisfy the target values are presented in Table 2.

5.2 Straight Track Performance

The performance of the re-centering NSD in high-speed trains is evaluated numerically with the same model used in the LQR controller analysis. Fig. 12 presents the response of the car body when a high-speed train with re-centering NSD travels on a straight track at 300 km/h. Three cases with different negative stiffness and damping coefficient combinations are evaluated (Case 1: $k_n = -315$ kN/m, $c_n = 5.2$ kNs/m; Case 2: $k_n = -216$ kN/m, $c_n = 20.8$ kNs/m; Case 1: $k_n = -105$ kN/m, $c_n = 36.4$ kNs/m). Fig. 12(a), 12(b), and 12(c) show the car body responses in the lateral, yaw, and roll

directions, respectively. As shown in these figures, the responses in all directions decrease as the strength of negative stiffness increases. When the negative stiffness increases from −105 kN/m to −315 kN/m, the peak car body accelerations in the lateral, yaw, and roll directions decrease from approximately 0.5 m/s^2 to 0.02 m/s^2, 0.1 m/s^2 to 0.007 rad/s^2, and 0.3 m/s^2 to 0.017 rad/s^2, respectively. Similar conclusions are drawn from the car body response in the frequency domain. As shown in Fig. 13(a), 13(b), and 13(c), the peak responses of PSD in the lateral, yaw, and roll directions decrease as the strength of the negative stiffness increases.

Although the re-centering NSD reduces the car body responses significantly, it does not affect the response of the bogies and wheelset. Table 3 summarizes the RMS values of train responses when the train is protected by a passive damper, an LQR controller, and a re-centering NSD. Except for the car body responses, the differences between the bogies and wheelset responses of the three methods are within 5%.

5.3 Curved Track Performance

The re-centering function ensures that the relative displacements between the car body and bogie are not amplified by negative stiffness. Fig. 15 presents the time history of relative displacement between the car body and leading bogie when a high-speed train travels on a curved track whose geometry is presented in Fig. 4(a). As shown in Fig. 15, all of the relative displacements of the train with a passive damper, an LQR ($\mathbf{R} = \mathbf{I} \times 10^{-6}$) controller, and a re-centering NSD ($k_n = -210$ kN/m) are approximately 13 cm. However, without the re-centering function, the relative displacement is amplified by negative stiffness to 27 cm (Fig. 15).

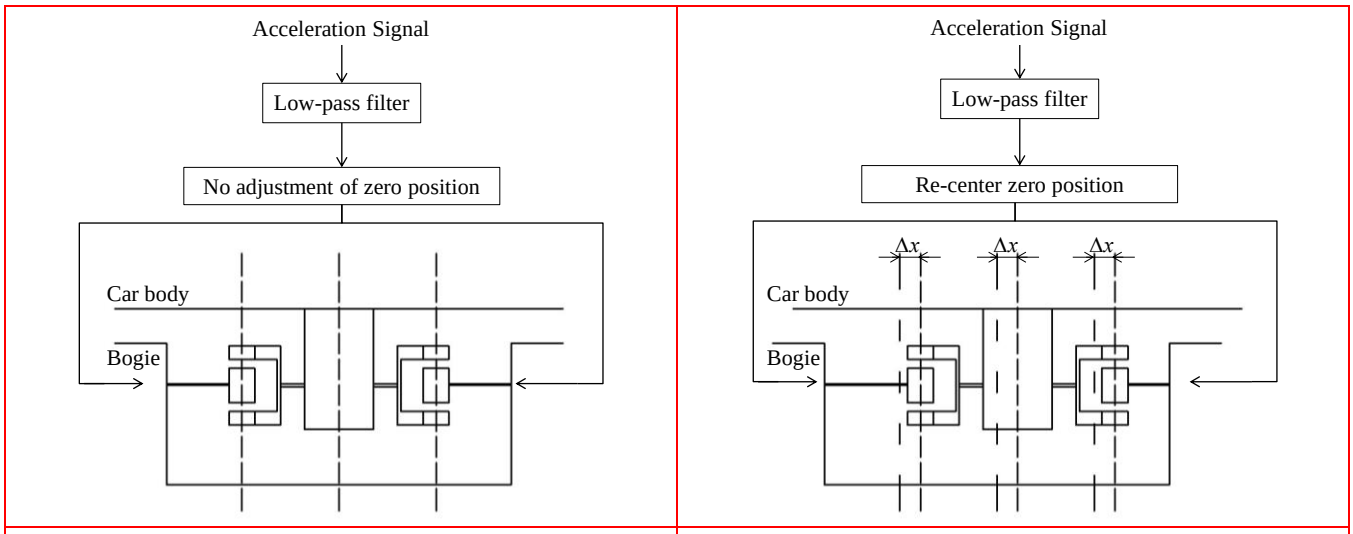

(a) On a straight track (b) On a curved track

Fig. 11 Principle of the re-centering function

Table 2 Magnet dimension for three levels of negative stiffness

Case No.	k_n (kN/m)	Static magnet			Moving magnet	
		outer radius (mm)	inner radius (mm)	thickness (mm)	radius (mm)	thickness (mm)
1	-315	40	31	80	30	80
2	-210	30	22	80	21	80
3	-105	20	11	80	10	80

Table 3 RMS of trai various control methods

Motion	Passive	LQR	NSD
		R=1×10-10	k_n=-315 kN/m
θ_{t2} (rad/s^2)	0.283953	0.24519	0.211214
y_{w1} (m/s^2)	8.772473	25.93056	8.883672
φ_{w1} (rad/s^2)	6.049266	4.049426	5.336823
y_{w2} (m/s^2)	8.633698	25.92741	8.800308

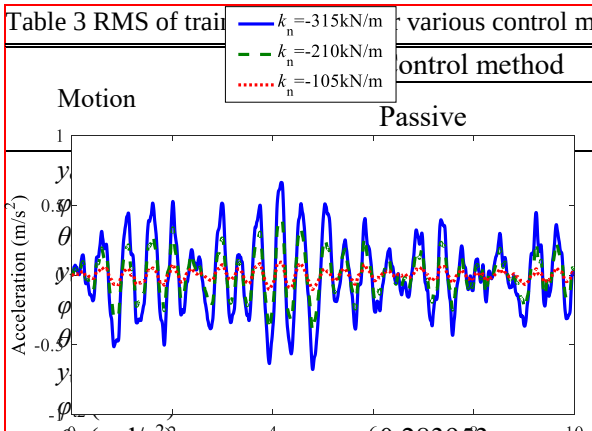

(a) Lateral accelerations

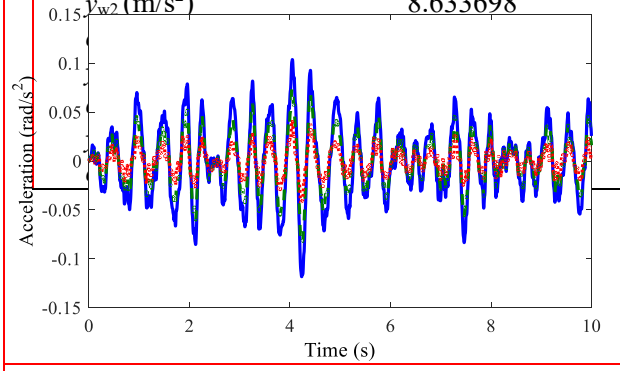

(b) Yaw accelerations

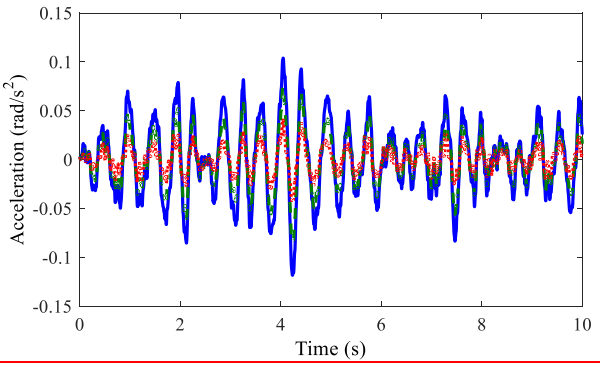

(c) Roll accelerations

Fig. 12 Time history of car body accelerations under random track irregularities

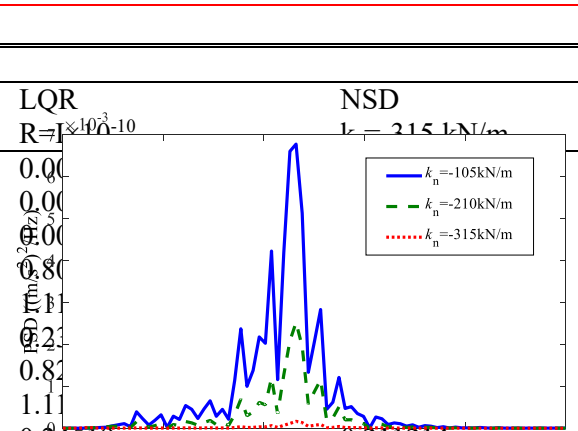

(a) Lateral accelerations

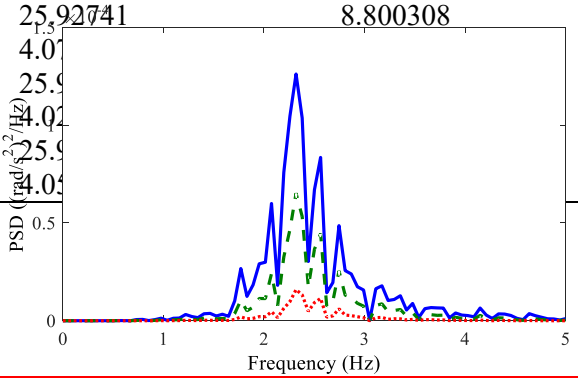

(b) Yaw accelerations

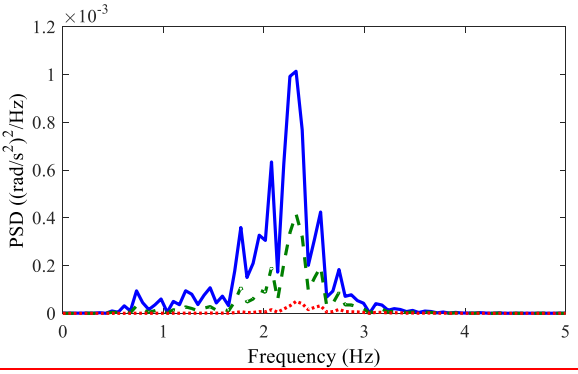

(c) Roll accelerations

Fig. 13 PSD of car body accelerations under random track irregularities

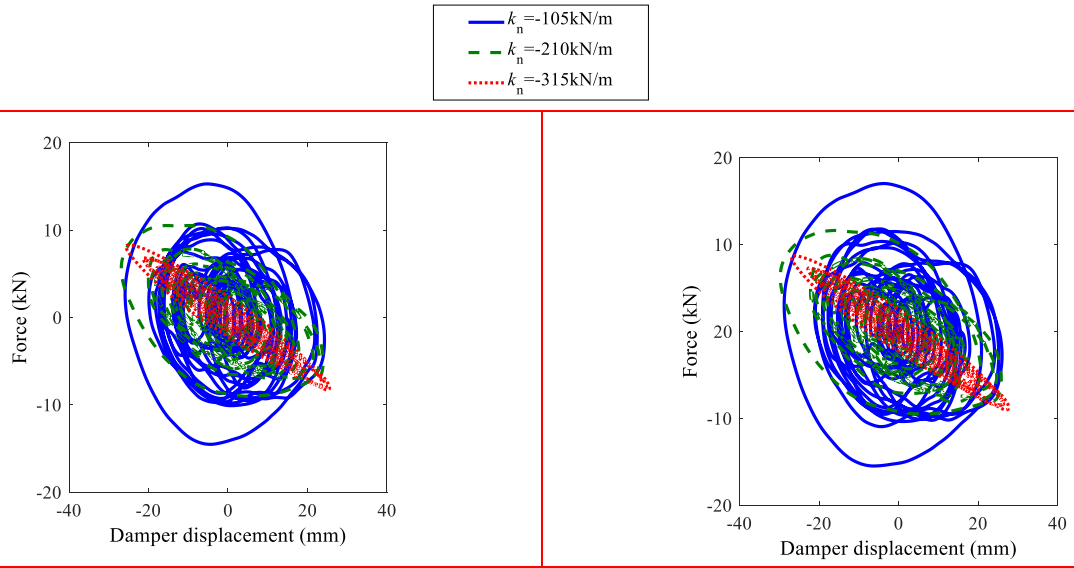

(a) Lead (b) Rear

Fig. 14 Control force vs. damper displacement of NSD

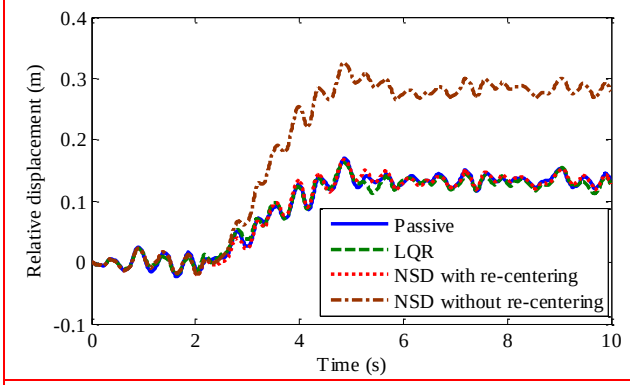

Fig. 15 Time history of relative displacement between the car body and lead bogie
(LQR: $\mathbf{R}=\mathbf{I}\times10^{-6}$, NSD: $k_n = -210$ kN/m)

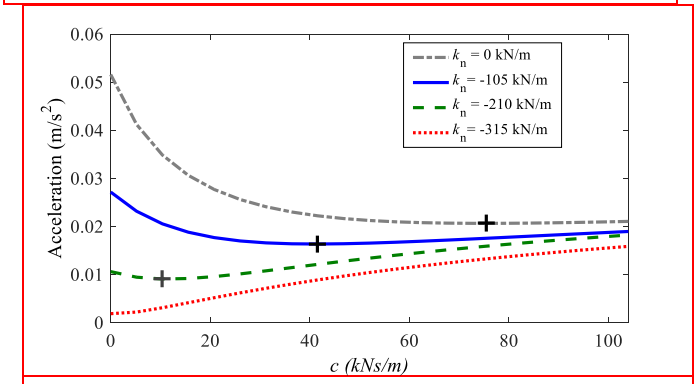

(a) V=100 km/h

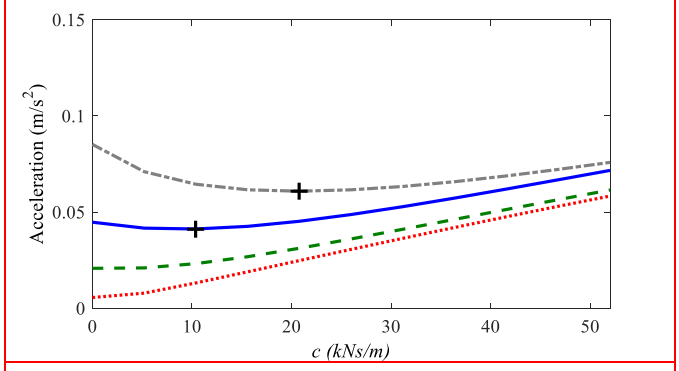

(b) V=200 km/h

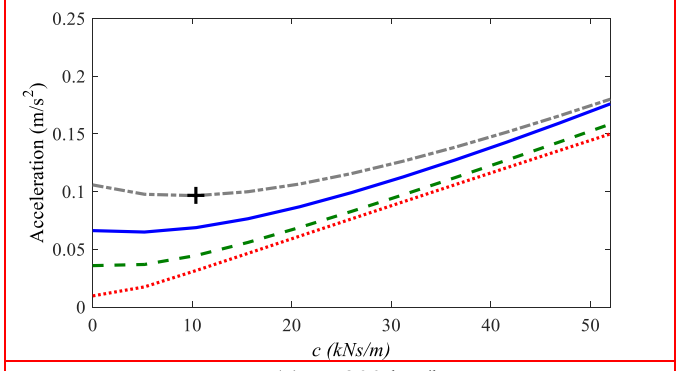

(c) V=300 km/h

Fig. 16 RMS of car body lateral accelerations of a high-speed train at various train speeds

5.4 Parametric Analysis

The performance of the re-centering NSD is determined by negative stiffness and damping coefficients. Fig. 16 presents the RMS lateral accelerations of the car body of a high-speed train with different negative stiffness values and damping coefficients. Fig. 16(a), 16(b), and 16(c) present the results when the high-speed train travels at 100, 200, and 300 km/h, respectively. The lowest point (as shown by the black cross in Fig. 16) of each curve corresponds to the optimal ride comfort performance and optimal damping coefficient. Without negative stiffness (k_n = 0), a small damping coefficient can provide good performance at a high traveling speed, whereas a large damping coefficient is effective at a low train speed. However, the introduction of negative stiffness weakens this speed-dependent trend. The optimal damping coefficient decreases as negative stiffness increases. When $k_n = -315$ kN/m, increasing the damping coefficient degrades the ride comfort at all three speeds. In general, the introduction of negative stiffness considerably reduces the RMS acceleration of the car body for different damping coefficients at all speeds. Adding strong negative stiffness to the second suspension is always beneficial for improving ride comfort, even when the damping coefficient is not optimally tuned.

5.5 Comparison with LQR

Fig. 18 and Fig. 19 summarize the RMS values of car body responses when the train is protected by a re-centering NSD and an LQR controller, respectively. The train speed is 300 km/h in this analysis. Previous parametric analysis results indicate that a strong negative stiffness coefficient corresponds to a small optimal damping coefficient. Further analysis reveals that the optimal damping coefficient decreases linearly with the increase in the negative stiffness coefficient at this speed, as presented in Fig. 17. Under this condition, the car body responses in all three directions decrease approximately linearly with negative stiffness (Fig. 18). Similarly, the car body responses of a high-speed train with an LQR controller decrease as the **R** value decreases (Fig. 19). However, the decrement ratio differs for different **R** values and motion directions (Fig. 19). According to Fig. 18 and Fig. 19, the NSD with sufficient negative stiffness can achieve comparable performances to an LQR controller. It shall also be pointed out that the simulation results of the high-speed train with an LQR controller are ideal. In practice, the sensing noise and the feedback delay may considerably degrade the performance of the LQR controller. However, the passive NSD is immune from such adverse effects.

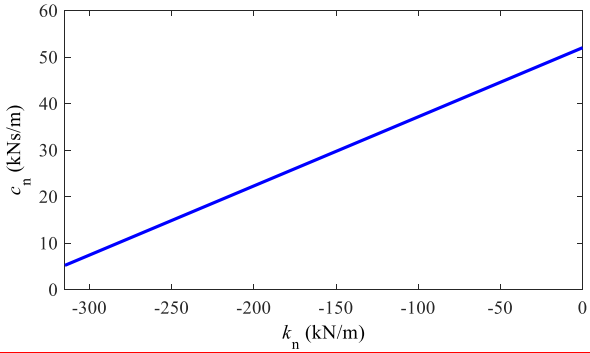

Fig. 17 Optimal relationship between negative stiffness and damping coefficients

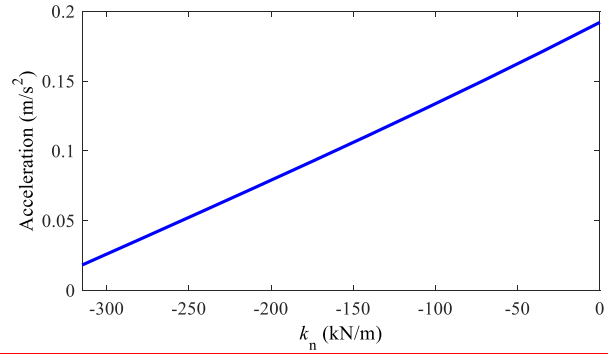

(a) Lateral accelerations

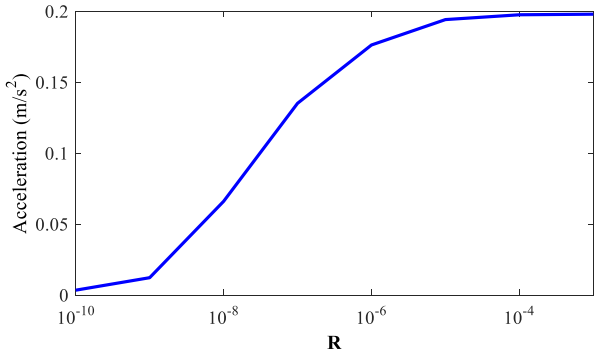

(a) Lateral accelerations

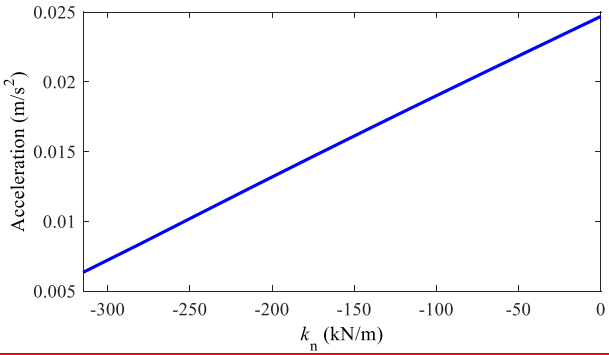

(b) Yaw accelerations

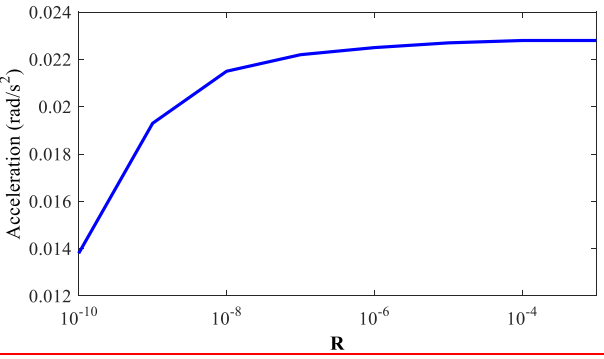

(b) Yaw accelerations

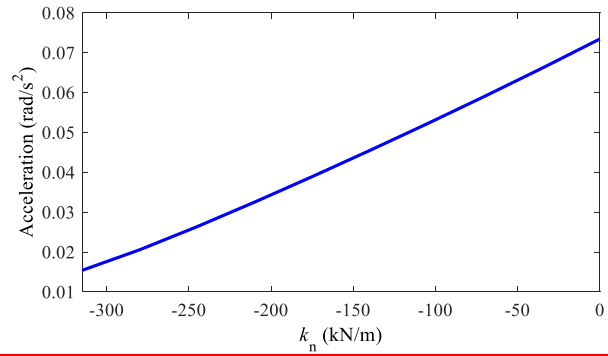

(c) Roll accelerations

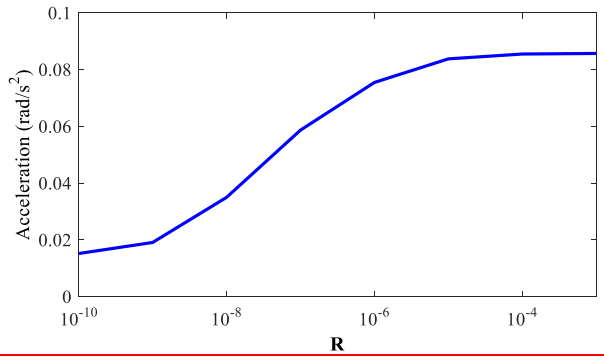

(c) Roll accelerations

Fig. 18 Car body response of a high-speed train with NSD at a traveling speed of 300 km/h

Fig. 19 Car body response of a high-speed train with an active LQR controller at a traveling speed of 300 km/h

6. Conclusion

This work evaluates the benefits of negative stiffness in the vibration control of high-speed trains and proposes a re-centering negative stiffness damper (NSD) for high-speed train suspensions. The numerical simulations reveal that the force–deformation relationship produced by active controllers (LQR) in high-speed trains possesses an obvious negative stiffness feature. As the control energy of the active controller increases, the controllers' performance improves, and the negative stiffness feature in their hysteresis loop becomes highly significant. To combine the high performance of active controllers and excellent robustness of passive dampers, a passive NSD with a re-centering function is proposed. In the proposed damper, passive negative stiffness is realized with a magnetic negative stiffness spring, and the re-centering function is realized by using a positioning shaft. The capability of NSD to improve ride comfort significantly is verified numerically, and the re-centering function can avoid large spring deflection when a train travels on a curved track.

Acknowledgement

The authors are grateful for the financial support from the Innovation and Technology Commission of the HKSAR Government to the Hong Kong Branch of National Rail Transit Electrification and Automation Engineering Technology Research Center (Project No. 1-BBY5) and from the Research Grants Council of Hong Kong through the GRF grant (Project No. PolyU 152222/14E). The findings and opinions expressed in this paper are solely those of the authors and are not necessarily the views of sponsors.

References

Allen, D. H. (1994). Active bumpstop hold-off device. *In Proc IMechE Conference Railtech* (Vol. **94**).

Asai, T., Spencer, B. F., Iemura, H., & Chang, C. M. (2013). Nature of seismic control force in acceleration feedback. *Structural Control and Health Monitoring*, **20**(5), 789-803.

Atray, V. S., & Roschke, P. N. (2004). Neuro‐Fuzzy Control of Railcar Vibrations Using Semiactive Dampers. *Computer‐Aided Civil and Infrastructure Engineering*, **19**(2), 81-92.

Balch, S. P., & Lakes, R. S. (2017). Lumped negative stiffness damper for absorption of flexural waves in a rod. *Smart Materials and Structures*, **26**(4), 045022.

Braghin, F., Bruni, S., & Resta, F. (2006). Active yaw damper for the improvement of railway vehicle stability and curving performances: simulations and experimental results. *Vehicle System Dynamics*, **44**(11), 857-869.

Bruni, S., & Resta, F. (2001). Active control of railway vehicles to avoid hunting instability. *In Advanced Intelligent Mechatronics, 2001. Proceedings. 2001 IEEE/ASME International Conference on* (Vol. **1**, pp. 231-236). IEEE.

Bruni, S., Goodall, R., Mei, T. X., & Tsunashima, H. (2007). Control and monitoring for railway vehicle dynamics. *Vehicle System Dynamics*, **45**(7-8), 743-779.

Chen, G., & Zhai, W. (1999). Numerical simulation of the stochastic process of railway track irregularities. *Journal of Southwest Jiaotong University*, **34**(2), 138-142.

Churchill, C. B., Shahan, D. W., Smith, S. P., Keefe, A. C., & McKnight, G. P. (2016). Dynamically variable negative stiffness structures. *Science advances*, **2**(2), e1500778.

Claus, H., & Schiehlen, W. (1998). Modeling and simulation of railway bogie structural vibrations. *Vehicle System Dynamics*, **29**(S1), 538-552.

Cortes, S., Allison, J., Morris, C., Haberman, M. R., Seepersad, C. C., & Kovar, D. (2017). Design, Manufacture, and Quasi-Static Testing of Metallic Negative Stiffness Structures within a Polymer Matrix. *Experimental Mechanics*, 1-9.

Dijkstra, K., Videc, B. P., & Huizinga, J. (1988). U.S. Patent No. 4,722,517. Washington, DC: U.S. Patent and Trademark Office.

Garivaltis, D. S., Garg, V. K., & D'souza, A. F. (1980). Dynamic response of a six-axle locomotive to random track inputs. *Vehicle System Dynamics*, **9**(3), 117-147.

Goodall, R. (1997). Active railway suspensions: Implementation status and technological trends. *Vehicle System Dynamics*, **28**(2-3), 87-117.

Goodall, R. M., & Kortüm, W. (2002). Mechatronic developments for railway vehicles of the future. *Control Engineering Practice*, **10**(8), 887-898.

He, Y., & McPhee, J. (2005). Multidisciplinary design optimization of mechatronic vehicles with active suspensions. *Journal of Sound and Vibration*, **283**(1), 217-241.

Høgsberg, J. (2011). The role of negative stiffness in semi‐active control of magneto‐rheological dampers. *Structural Control and Health Monitoring*, **18**(3), 289-304.

Iemura, H., & Pradono, M. H. (2002). Passive and semi‐active seismic response control of a cable‐stayed bridge. *Structural Control and Health Monitoring*, **9**(3), 189-204.

Iemura, H., & Pradono, M. H. (2005). Simple algorithm for semi‐active seismic response control of cable‐stayed bridges. *Earthquake engineering & structural dynamics*, **34**(4‐5), 409-423.

Iemura, H., Igarashi, A., Pradono, M. H., & Kalantari, A. (2006). Negative stiffness friction damping for seismically isolated structures. *Structural control and health monitoring*, **13**(2‐3), 775-791.

Iemura, H., & Pradono, M. H. (2009). Advances in the development of pseudo‐negative‐stiffness dampers for seismic response control. *Structural Control and Health Monitoring*, **16**(7‐8), 784-799.

Kalathur, H., & Lakes, R. S. (2013). Column dampers with negative stiffness: high damping at small amplitude. *Smart Materials and Structures*, **22**(8), 084013.

Lee, C. M., Goverdovskiy, V. N., & Temnikov, A. I. (2007). Design of springs with "negative" stiffness to improve vehicle driver vibration isolation. *Journal of Sound and Vibration*, **302**(4), 865-874.

Le, T. D., & Ahn, K. K. (2011). A vibration isolation system in low frequency excitation region using negative stiffness structure for vehicle seat. *Journal of Sound and Vibration*, **330**(26), 6311-6335.

Lee, C. M., & Goverdovskiy, V. N. (2012). A multi-stage high-speed railroad vibration isolation system with "negative" stiffness. *Journal of Sound and Vibration*, **331**(4), 914-921.

Lee, C. M., Goverdovskiy, V. N., Sim, C. S., & Lee, J. H. (2016). Ride comfort of a high-speed train through the structural upgrade of a bogie suspension. *Journal of Sound and Vibration*, **361**, 99-107.

Li, H., Liu, M., & Ou, J. (2008). Negative stiffness characteristics of active and semi‐active control systems for stay cables. *Structural Control and Health Monitoring*, **15**(2), 120-142.

Li, Z., Ni, Y. Q., Dai, H., & Ye, S. (2013). Viscoelastic plastic continuous physical model of a magnetorheological damper applied in the high speed train. *Science China Technological Sciences*, **56**(10), 2433-2446.

Li, D. Y., Song, Y. D., & Cai, W. C. (2015). Neuro-adaptive fault-

tolerant approach for active suspension control of high-speed trains. *IEEE Transactions on Intelligent Transportation Systems*, **16**(5), 2446-2456.

Liao, W. H., & Wang, D. H. (2003). Semiactive vibration control of train suspension systems via magnetorheological dampers. *Journal of intelligent material systems and structures*, **14**(3), 161-172.

Liu, Y., Yu, D. P., & Yao, J. (2016). Design of an adjustable cam based constant force mechanism. *Mechanism and Machine Theory*, 103, 85-97.

Mellado, A. C., Casanueva, C., Vinolas, J., & Giménez, J. G. (2009). A lateral active suspension for conventional railway bogies. *Vehicle System Dynamics*, **47**(1), 1-14.

Ni, Y. Q., Ye, S. Q., & Song, S. D. (2016). An experimental study on constructing MR secondary suspension for high-speed trains to improve lateral ride comfort. *Smart Structures and Systems*, **18**(1), 53-74.

O'Neill, H. R., & Wale, G. D. (1994). Semi-active suspension improves rail vehicle ride. *Computing & Control Engineering Journal*, **5**(4), 183-188.

Orukpe, P. E., Zheng, X., Jaimoukha, I. M., Zolotas, A. C., & Goodall, R. M. (2008). Model predictive control based on mixed ℋ2/ℋ∞ control approach for active vibration control of railway vehicles. *Vehicle System Dynamics*, **46**(S1), 151-160.

Orvnäs, A., Stichel, S., & Persson, R. (2010). Ride comfort improvements in a high-speed train with active secondary suspension. *Journal of Mechanical Systems for Transportation and Logistics*, **3**(1), 206-215.

Orvnäs, A., Stichel, S., & Persson, R. (2011). Active lateral secondary suspension with H∞ control to improve ride comfort: simulations on a full-scale model. *Vehicle System Dynamics*, **49**(9), 1409-1422.

Pasala, D. T. R., Sarlis, A. A., Nagarajaiah, S., Reinhorn, A. M., Constantinou, M. C., & Taylor, D. (2012). Adaptive negative stiffness: new structural modification approach for seismic protection. *Journal of Structural Engineering*, **139**(7), 1112-1123.

Pearson, J. T., Goodall, R. M., & Pratt, I. (1998). Control system studies of an active anti-roll bar tilt system for railway vehicles. *Proceedings of the Institution of Mechanical Engineers, Part F: Journal of Rail and Rapid Transit*, **212**(1), 43-60.

Peiffer, A., Storm, S., Röder, A., Maier, R., & Frank, P. G. (2004). Active vibration control for high speed train bogies. *Smart materials and structures*, **14**(1), 1.

Platus, D. L., & Ferry, D. K. (2007). Negative-stiffness vibration isolation improves reliability of nanoinstrumentation. *Laser Focus World*, **43**(10), 107.

Pratt, I., & Goodall, R. (1997, June). Controlling the ride quality of the central portion of a high-speed railway vehicle. *In American Control Conference, 1997. Proceedings of the 1997* (Vol. 1, pp. 719-723). IEEE.

Sasaki, K., Kamoshita, S., & Enomoto, M. (1994, September). A design and bench test of multi-modal active suspension of railway vehicle. *In Industrial Electronics, Control and Instrumentation, 1994. IECON'94., 20th International Conference on* (Vol. 3, pp. 2011-2016). IEEE.

Shi, X., & Zhu, S. (2015). Magnetic negative stiffness dampers. *Smart Materials and Structures*, **24**(7), 072002.

Shi, X., Zhu, S., Li, J. Y., & Spencer Jr, B. F. (2016). Dynamic behavior of stay cables with passive negative stiffness dampers. *Smart Materials and Structures*, **25**(7), 075044.

Shi, X., Zhu, S., & Spencer Jr, B. F. (2017). Experimental study on passive negative stiffness damper for cable vibration mitigation, *Journal of Engineering Mechanics*,**143**(9), 04017070.

Shi, X., & Zhu, S. (2017). Simulation and optimization of magnetic negative stiffness dampers. *Sensors and Actuators A: Physical*. **259**, 14-33.

Shimamune, R., & Tanifuji, K. (1995, July). Application of oil-hydraulic actuator for active suspension of railway vehicle: experimental study. *In SICE'95. Proceedings of the 34th SICE Annual Conference. International Session Papers* (pp. 1335-1340). IEEE.

Sun, S., Deng, H., Li, W., Du, H., Ni, Y. Q., Zhang, J., & Yang, J. (2013). Improving the critical speeds of high-speed trains using magnetorheological technology. *Smart Materials and Structures*, **22**(11), 115012.

Sun, T., Lai, Z., Nagarajaiah, S., & Li, H. N. (2017). Negative stiffness device for seismic protection of smart base isolated benchmark building. *Structural Control and Health Monitoring*.

Tanifuji, K. (1998). A prediction of wheel/rail lateral force induced by actively controlled suspension for high speed railway vehicles. *Vehicle System Dynamics*, **29**(S1), 367-379.

Tanifuji, K., Koizumi, S., & Shimamune, R. H. (2002). Mechatronics in Japanese rail vehicles: active and semi-active suspensions. *Control Engineering Practice*, **10**(9), 999-1004.

Wang, D. H., & Liao, W. H. (2009a). Semi-active suspension systems for railway vehicles using magnetorheological dampers. Part I: system integration and modelling. *Vehicle System Dynamics*, **47**(11), 1305-1325.

Wang, D. H., & Liao, W. H. (2009b). Semi-active suspension systems for railway vehicles using magnetorheological dampers. Part II: simulation and analysis. *Vehicle System Dynamics*, **47**(12), 1439-1471.

Weber, F., Boston, C., & Maślanka, M. (2010). An adaptive tuned mass damper based on the emulation of positive and negative stiffness with an MR damper. *Smart Materials and Structures*, **20**(1), 015012.

Weber, F., & Boston, C. (2011). Clipped viscous damping with negative stiffness for semi-active cable damping. Smart *Materials and Structures*, **20**(4), 045007.

Yang, J., Li, J., & Du, Y. (2006, August). Adaptive fuzzy control of lateral semi-active suspension for high-speed railway vehicle. *In International Conference on Intelligent Computing* (pp. 1104-1115). Springer Berlin Heidelberg.

Yang, J., Xiong, Y. P., & Xing, J. T. (2013). Dynamics and power flow behaviour of a nonlinear vibration isolation system with a negative stiffness mechanism. *Journal of sound and vibration*, **332**(1), 167-183.

Yoshimura, T., Edokoro, K., & Ananthanarayana, N. (1993). An active suspension model for rail/vehicle systems with preview and stochastic optimal control. *Journal of sound and vibration*, **166**(3), 507-519.

Zhou, R., Zolotas, A., & Goodall, R. (2010, June). LQG control for the integrated tilt and active lateral secondary suspension in high speed railway vehicles. *In Control and Automation (ICCA), 2010 8th IEEE International Conference on* (pp. 16-21). IEEE.

Zong, L. H., Gong, X. L., Xuan, S. H., & Guo, C. Y. (2013). Semi-active H∞ control of high-speed railway vehicle suspension with magnetorheological dampers. *Vehicle System Dynamics*, **51**(5), 600-626.

Appendix

The governing equations of the 17-DOF high-speed train model developed by Zong et al. (2013) are briefly described in this appendix.

Car body dynamics

$$
\begin{aligned}
&M_c\ddot{y}_c + K_{2y}\left(y_c + l\varphi_c - h_1\theta_c - y_{t1} - h_3\theta_{t1}\right)\\
&+C_{2y}\left(\dot{y}_c + l\dot{\varphi}_c - h_2\dot{\theta}_c - \dot{y}_{t1} - h_5\dot{\theta}_{t1}\right)\\
&+K_{2y}\left(y_c - l\varphi_c - h_1\theta_c - y_{t2} - h_3\theta_{t2}\right)\\
&+C_{2y}\left(\dot{y}_c - l\dot{\varphi}_c - h_2\dot{\theta}_c - \dot{y}_{t2} - h_5\dot{\theta}_{t2}\right)\\
&= u_1 + u_2\\
&J_{cz}\ddot{\varphi}_c + K_{2y}l\left(y_c + l\varphi_c - h_1\theta_c - y_{t1} - h_3\theta_{t1}\right)\\
&+C_{2y}l\left(\dot{y}_c + l\dot{\varphi}_c - h_2\dot{\theta}_c - \dot{y}_{t1} - h_5\dot{\theta}_{t1}\right)\\
&-K_{2y}l\left(y_c - l\varphi_c - h_1\theta_c - y_{t2} - h_3\theta_{t2}\right)\\
&-C_{2y}l\left(\dot{y}_c - l\dot{\varphi}_c - h_2\dot{\theta}_c - \dot{y}_{t2} - h_5\dot{\theta}_{t2}\right)\\
&+K_{2x}b_2^2\left(\varphi_c - \varphi_{t1}\right) + C_{2x}b_3^2\left(\dot{\varphi}_c - \dot{\varphi}_{t1}\right)\\
&+K_{2x}b_2^2\left(\varphi_c - \varphi_{t2}\right) + C_{2x}b_3^2\left(\dot{\varphi}_c - \dot{\varphi}_{t2}\right)\\
&= u_1 l - u_2 l\\
&J_{cx}\ddot{\theta}_c - K_{2y}h_1\left(y_c + l\varphi_c - h_1\theta_c - y_{t1} - h_3\theta_{t1}\right)\\
&-C_{2y}h_2\left(\dot{y}_c + l\dot{\varphi}_c - h_2\dot{\theta}_c - \dot{y}_{t1} - h_5\dot{\theta}_{t1}\right)\\
&-K_{2y}h_1\left(y_c - l\varphi_c - h_1\theta_c - y_{t2} - h_3\theta_{t2}\right)\\
&-C_{2y}h_2\left(\dot{y}_c - l\dot{\varphi}_c - h_2\dot{\theta}_c - \dot{y}_{t2} - h_5\dot{\theta}_{t2}\right)\\
&+K_{2z}b_2^2\left(\theta_c - \theta_{t1}\right) + C_{2z}b_3^2\left(\dot{\theta}_c - \dot{\theta}_{t1}\right)\\
&+K_{2z}b_2^2\left(\theta_c - \theta_{t2}\right) + C_{2x}b_3^2\left(\dot{\theta}_c - \dot{\theta}_{t1}\right)\\
&= -u_1 h_2 - u_2 h_2
\end{aligned}
$$

Bogie dynamics

$$
\begin{aligned}
&M_t\ddot{y}_{t1} - K_{2y}\left(y_c + l\varphi_c - h_1\theta_c - y_{t1} - h_3\theta_{t1}\right)\\
&-C_{2y}\left(\dot{y}_c + l\dot{\varphi}_c - h_2\dot{\theta}_c - \dot{y}_{t1} - h_5\dot{\theta}_{t1}\right)\\
&+K_{1y}\left(y_{t1} + l_1\varphi_{t1} - h_4\theta_{t1} - y_{w1}\right)\\
&+C_{1y}\left(\dot{y}_{t1} + l_1\dot{\varphi}_{t1} - h_4\dot{\theta}_{t1} - \dot{y}_{w1}\right)\\
&+K_{1y}\left(y_{t1} - l_1\varphi_{t1} - h_4\theta_{t1} - y_{w2}\right)\\
&+C_{1y}\left(\dot{y}_{t1} - l_1\dot{\varphi}_{t1} - h_4\dot{\theta}_{t1} - \dot{y}_{w2}\right)\\
&= -u_1\\
&M_t\ddot{y}_{t2} - K_{2y}\left(y_c - l\varphi_c - h_1\theta_c - y_{t2} - h_3\theta_{t2}\right)\\
&-C_{2y}\left(\dot{y}_c - l\dot{\varphi}_c - h_2\dot{\theta}_c - \dot{y}_{t2} - h_5\dot{\theta}_{t2}\right)\\
&+K_{1y}\left(y_{t2} + l_1\varphi_{t2} - h_4\theta_{t2} - y_{w3}\right)\\
&+C_{1y}\left(\dot{y}_{t2} + l_1\dot{\varphi}_{t2} - h_4\dot{\theta}_{t2} - \dot{y}_{w3}\right)\\
&+K_{1y}\left(y_{t2} - l_1\varphi_{t2} - h_4\theta_{t2} - y_{w4}\right)\\
&+C_{1y}\left(\dot{y}_{t2} - l_1\dot{\varphi}_{t2} - h_4\dot{\theta}_{t2} - \dot{y}_{w4}\right)\\
&= -u_2\\
&J_{tz}\ddot{\varphi}_{t1} - K_{2x}b_2^2\left(\varphi_c - \varphi_{t1}\right) - C_{2x}b_3^2\left(\dot{\varphi}_c - \dot{\varphi}_{t1}\right)\\
&+K_{1y}l_1\left(y_{t1} + l_1\varphi_{t1} - h_4\theta_{t1} - y_{w1}\right)\\
&+C_{1y}l_1\left(\dot{y}_{t1} + l_1\dot{\varphi}_{t1} - h_4\dot{\theta}_{t1} - \dot{y}_{w1}\right)\\
&-K_{1y}l_1\left(y_{t1} - l_1\varphi_{t1} - h_4\theta_{t1} - y_{w2}\right)\\
&-C_{1y}l_1\left(\dot{y}_{t1} - l_1\dot{\varphi}_{t1} - h_4\dot{\theta}_{t1} - \dot{y}_{w2}\right)\\
&+K_{1x}b_1^2\left(\varphi_{t1} - \varphi_{w1}\right) + C_{1x}b_1^2\left(\dot{\varphi}_{t1} - \dot{\varphi}_{w1}\right)\\
&+K_{1x}b_1^2\left(\varphi_{t1} - \varphi_{w2}\right) + C_{1x}b_1^2\left(\dot{\varphi}_{t1} - \dot{\varphi}_{w2}\right) = 0\\
&J_{tz}\ddot{\varphi}_{t2} - K_{2x}b_2^2\left(\varphi_c - \varphi_{t2}\right) - C_{2x}b_3^2\left(\dot{\varphi}_c - \dot{\varphi}_{t2}\right)\\
&+K_{1y}l_1\left(y_{t2} + l_1\varphi_{t2} - h_4\theta_{t2} - y_{w3}\right)\\
&+C_{1y}l_1\left(\dot{y}_{t2} + l_1\dot{\varphi}_{t2} - h_4\dot{\theta}_{t2} - \dot{y}_{w3}\right)\\
&-K_{1y}l_1\left(y_{t2} - l_1\varphi_{t2} - h_4\theta_{t2} - y_{w4}\right)\\
&-C_{1y}l_1\left(\dot{y}_{t2} - l_1\dot{\varphi}_{t2} - h_4\dot{\theta}_{t2} - \dot{y}_{w4}\right)\\
&+K_{1x}b_1^2\left(\varphi_{t2} - \varphi_{w3}\right) + C_{1x}b_1^2\left(\dot{\varphi}_{t2} - \dot{\varphi}_{w3}\right)\\
&+K_{1x}b_1^2\left(\varphi_{t2} - \varphi_{w4}\right) + C_{1x}b_1^2\left(\dot{\varphi}_{t2} - \dot{\varphi}_{w4}\right) = 0\\
&J_{tx}\ddot{\theta}_{t1} - K_{2y}h_3\left(y_c + l\varphi_c - h_1\theta_c - y_{t1} - h_3\theta_{t1}\right)\\
&-C_{2y}h_5\left(\dot{y}_c + l\dot{\varphi}_c - h_2\dot{\theta}_c - \dot{y}_{t1} - h_5\dot{\theta}_{t1}\right)\\
&-K_{2z}b_2^2\left(\theta_c - \theta_{t1}\right) - C_{2z}b_3^2\left(\dot{\theta}_c - \dot{\theta}_{t1}\right)\\
&-K_{1y}h_4\left(y_{t1} + l_1\varphi_{t1} - h_4\theta_{t1} - y_{w1}\right)\\
&-C_{1y}h_4\left(\dot{y}_{t1} - l_1\dot{\varphi}_{t1} - h_4\dot{\theta}_{t1} - \dot{y}_{w1}\right)\\
&-K_{1y}h_4\left(y_{t1} - l_1\varphi_{t1} - h_4\theta_{t1} - y_{w2}\right)\\
&-C_{1y}h_4\left(\dot{y}_{t1} - l_1\dot{\varphi}_{t1} - h_4\dot{\theta}_{t1} - \dot{y}_{w2}\right)\\
&+2K_{1z}b_1^2\theta_{t1} + 2C_{1z}b_1^2\dot{\theta}_{t1} = -u_1 h_5
\end{aligned}
$$

$$J_{tx}\ddot{\theta}_{t2}-K_{2y}h_3\left(y_c-l\varphi_c-h_1\theta_c-y_{t2}-h_3\theta_{t2}\right)$$
$$-C_{2y}h_5\left(\dot{y}_c-l\dot{\varphi}_c-h_2\dot{\theta}_c-\dot{y}_{t2}-h_5\dot{\theta}_{t2}\right)$$
$$-K_{2z}b_2^2\left(\theta_c-\theta_{t2}\right)-C_{2z}b_3^2\left(\dot{\theta}_c-\dot{\theta}_{t2}\right)$$
$$-K_{1y}h_4\left(y_{t2}+l_1\varphi_{t2}-h_4\theta_{t2}-y_{w3}\right)$$
$$-C_{1y}h_4\left(\dot{y}_{t2}-l_1\dot{\varphi}_{t2}-h_4\dot{\theta}_{t2}-\dot{y}_{w3}\right)$$
$$-K_{1y}h_4\left(y_{t2}-l_1\varphi_{t2}-h_4\theta_{t2}-y_{w4}\right)$$
$$-C_{1y}h_4\left(\dot{y}_{t2}-l_1\dot{\varphi}_{t2}-h_4\dot{\theta}_{t2}-\dot{y}_{w4}\right)$$
$$+2K_{1z}b_1^2\theta_{t2}+2C_{1z}b_1^2\dot{\theta}_{t2}=-u_2h_5$$

Wheelset dynamics

$$M_w\ddot{y}_{w1}-K_{1y}\left(y_{t1}+l_1\varphi_{t1}-h_4\theta_{t1}-y_{w1}\right)$$
$$-C_{1y}\left(\dot{y}_{t1}+l_1\dot{\varphi}_{t1}-h_4\dot{\theta}_{t1}-\dot{y}_{w1}\right)$$
$$+2f_{22}\left[\frac{\dot{y}_{w1}}{V}\left(1+\frac{\sigma r_0}{b}\right)-\varphi_{w1}\right]+K_{gy}y_{w1}$$
$$=2f_{22}\left(\frac{\sigma r_0}{Vb}\dot{y}_{a1}+\frac{\sigma r_0^2}{Vb}\dot{\theta}_{cl1}\right)$$
$$+K_{gy}\left(y_{a1}+r_0\theta_{cl1}\right)$$
$$M_w\ddot{y}_{w2}-K_{1y}\left(y_{t1}-l_1\varphi_{t1}-h_4\theta_{t1}-y_{w2}\right)$$
$$-C_{1y}\left(\dot{y}_{t1}-l_1\dot{\varphi}_{t1}-h_4\dot{\theta}_{t1}-\dot{y}_{w2}\right)$$
$$+2f_{22}\left[\frac{\dot{y}_{w2}}{V}\left(1+\frac{\sigma r_0}{b}\right)-\varphi_{w2}\right]+K_{gy}y_{w2}$$
$$=2f_{22}\left(\frac{\sigma r_0}{Vb}\dot{y}_{a2}+\frac{\sigma r_0^2}{Vb}\dot{\theta}_{cl2}\right)$$
$$+K_{gy}\left(y_{a2}+r_0\theta_{cl2}\right)$$
$$M_w\ddot{y}_{w3}-K_{1y}\left(y_{t2}+l_1\varphi_{t2}-h_4\theta_{t2}-y_{w3}\right)$$
$$-C_{1y}\left(\dot{y}_{t2}+l_1\dot{\varphi}_{t2}-h_4\dot{\theta}_{t2}-\dot{y}_{w3}\right)$$
$$+2f_{22}\left[\frac{\dot{y}_{w3}}{V}\left(1+\frac{\sigma r_0}{b}\right)-\varphi_{w3}\right]+K_{gy}y_{w3}$$
$$=2f_{22}\left(\frac{\sigma r_0}{Vb}\dot{y}_{a3}+\frac{\sigma r_0^2}{Vb}\dot{\theta}_{cl3}\right)$$
$$+K_{gy}\left(y_{a3}+r_0\theta_{cl3}\right)$$
$$M_w\ddot{y}_{w4}-K_{1y}\left(y_{t2}-l_1\varphi_{t2}-h_4\theta_{t2}-y_{w4}\right)$$
$$-C_{1y}\left(\dot{y}_{t2}-l_1\dot{\varphi}_{t2}-h_4\dot{\theta}_{t2}-\dot{y}_{w4}\right)$$
$$+2f_{22}\left[\frac{\dot{y}_{w4}}{V}\left(1+\frac{\sigma r_0}{b}\right)-\varphi_{w4}\right]+K_{gy}y_{w4}$$
$$=2f_{22}\left(\frac{\sigma r_0}{Vb}\dot{y}_{a4}+\frac{\sigma r_0^2}{Vb}\dot{\theta}_{cl4}\right)$$
$$+K_{gy}\left(y_{a4}+r_0\theta_{cl4}\right)$$
$$J_{wz}\ddot{\varphi}_{w1}+K_{1x}b_1^2\left(\varphi_{w1}-\varphi_{t1}\right)$$
$$+2f_{11}\left[\frac{b\lambda_e}{r_0}y_{w1}+\frac{b^2}{V}\dot{\varphi}_{w1}\right]-K_{g\varphi}\varphi_{w1}$$
$$=2f_{11}\frac{b\lambda_e}{r_0}\left(y_{a1}+r_0\theta_{cl1}\right)$$
$$J_{wz}\ddot{\varphi}_{w2}+K_{1x}b_1^2\left(\varphi_{w2}-\varphi_{t1}\right)$$
$$+2f_{11}\left[\frac{b\lambda_e}{r_0}y_{w2}+\frac{b^2}{V}\dot{\varphi}_{w2}\right]-K_{g\varphi}\varphi_{w2}$$
$$=2f_{11}\frac{b\lambda_e}{r_0}\left(y_{a2}+r_0\theta_{cl2}\right)$$
$$J_{wz}\ddot{\varphi}_{w3}+K_{1x}b_1^2\left(\varphi_{w3}-\varphi_{t2}\right)$$
$$+2f_{11}\left[\frac{b\lambda_e}{r_0}y_{w3}+\frac{b^2}{V}\dot{\varphi}_{w3}\right]-K_{g\varphi}\varphi_{w3}$$
$$=2f_{11}\frac{b\lambda_e}{r_0}\left(y_{a3}+r_0\theta_{cl3}\right)$$
$$J_{wz}\ddot{\varphi}_{w4}+K_{1x}b_1^2\left(\varphi_{w4}-\varphi_{t2}\right)$$
$$+2f_{11}\left[\frac{b\lambda_e}{r_0}y_{w4}+\frac{b^2}{V}\dot{\varphi}_{w4}\right]-K_{g\varphi}\varphi_{w4}$$
$$=2f_{11}\frac{b\lambda_e}{r_0}\left(y_{a4}+r_0\theta_{cl4}\right)$$

where k_{gy} is the lateral gravitational stiffness and $k_{g\varphi}$ is the yaw gravitational stiffness which is given by:

$$K_{gy}=\frac{W\lambda_e}{b}$$
$$K_{g\varphi}=-Wb\lambda_e$$